

PAPER

# Theory of microstructured polymer–electrolyte artificial muscles

To cite this article: Zachary A H Goodwin *et al* 2018 *Smart Mater. Struct.* **27** 075056

View the [article online](#) for updates and enhancements.

## Related content

- [Statics and dynamics of electroactuation with single-charge-carrier ionomers](#)  
Alpha A Lee, Ralph H Colby and Alexei A Kornyshev
- [Smart contact oscillations by IPMCs](#)  
H Asanuma, K Asaka, J Su et al.
- [Sensorless position estimator applied to nonlinear IPMC model](#)  
Jakub Bernat and Jakub Kolota

# Theory of microstructured polymer–electrolyte artificial muscles

Zachary A H Goodwin<sup>1,2,3</sup> , Michael Eikerling<sup>3,4</sup> , Hartmut Löwen<sup>3</sup>  and Alexei A Kornyshev<sup>2,3</sup> 

<sup>1</sup>Department of Physics, CDT Theory and Simulation of Materials, Imperial College London, South Kensington Campus, London SW7 2AZ, United Kingdom

<sup>2</sup>Department of Chemistry, Imperial College London, South Kensington Campus, London SW7 2AZ, United Kingdom

<sup>3</sup>Institute of Theoretical Physics, Heinrich-Heine University of Düsseldorf, Universitätsstr. 1, D-40225 Düsseldorf, Germany

<sup>4</sup>Department of Chemistry, Simon Fraser University, 8888 University Drive, Burnaby, BC, V5A 1S6, Canada

E-mail: [a.kornyshev@imperial.ac.uk](mailto:a.kornyshev@imperial.ac.uk)

Received 12 December 2017, revised 6 April 2018

Accepted for publication 4 May 2018

Published 22 June 2018



CrossMark

## Abstract

Ionic electroactuator beams are promising systems for artificial muscles in microrobotics. Here a theory is developed to investigate one promising class of such systems, which employs flexible volume-filling electrodes impregnated with polymer–electrolyte. The theory provides analytical formulae for the equilibrium beam curvature as a function of voltage and structure-related operational parameters. It predicts a possible enhancement of beam curvature by orders of magnitude over that of flat electrodes. Volume-filling electrodes thus constitute one of the ‘strongest’ architectures for voltage-induced movement. Approximate expressions for the dynamics of tandem pore charging and beam deflection are developed to determine the maximum pore length that still warrants a sufficiently fast response time (up to 1 s). Upper bounds on applied voltage and response time constrain the maximal device thickness and curvature, and therefore, the resulting work such a device can perform.

Supplementary material for this article is available [online](#)

Keywords: polymer–electrolyte electroactuator, porous electrodes, electrical double layer, ion transport, transmission line, artificial muscles

(Some figures may appear in colour only in the online journal)

## 1. Introduction

Ionic polymer metal composites (IPMCs) have, for a long time, attracted attention as prototypes for artificial muscles [1–18]. Beam elasticity and mobility of internal (ionic and solvent) species permits these composites to curve under an applied voltage; thereby converting electrical energy into mechanical work [1–18]. Ideally the polymer–electrolyte film, sandwiched between two thin electrodes, conducts one sort of ions [9–13], while counterions are immobilised at the surfaces of hydrophobic polymer domains [9–13]. The prototypical ionomer material is Nafion<sup>®</sup> in which the mobile protons have been exchanged for large cations [9, 10, 14, 15].

In polymer–electrolyte elastomers, when the upper electrode is polarised negatively, cations form a double layer there, leaving the space charge at the lower electrode cation-depleted [9–12]. In the cation-enriched double layer, the concentration of cations can increase ultimately to the maximal possible concentration, limited by the excluded volume effect. On the other hand, in the cation-depleted region, density of negative charge cannot drop lower than the density of residual anionic groups (SO<sub>3</sub><sup>-</sup> in Nafion<sup>®</sup> [9]) [19]. This leads to a specific potential distribution and capacitance-voltage dependence, reminiscent of p-type semiconductors. The excess of cations induces volumetric stress in the cation-enriched region, which causes it to

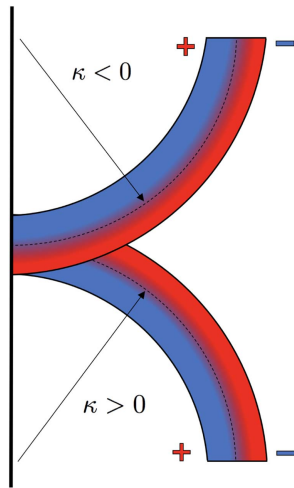


**Figure 1.** Depiction of IPMC beam curving under applied voltage. Red regions represent areas of cation enrichment and blue regions of cation depletion in volume-filling electrodes. Arrows and curvature,  $\kappa$ , indicate the sign convention utilised throughout.

swell; whereas the cation-depleted region at the lower electrode shrinks. Thus such redistribution of cations and water causes the beam to bend down [9–12], as depicted in figure 1.

Electroactuators composed of polymer–electrolyte films with flat electrodes [2–13] have been studied since the early 1990s [1] (see [20] for a detailed review). In such configurations, the cation-enriched and cation-depleted double layers are localised in narrow regions close to the corresponding electrodes [9, 10, 12]. This design leaves a large proportion of polymer–electrolyte film unperturbed and thus inactive in producing volumetric stress.

Improved actuation has already been achieved through volume-filling electrode architectures [21–38]. For example, carbon nanotube forests and porous metal particle electrodes [31–33] have experimentally demonstrated enhanced responses over flat electrodes. The same principle to improve the actuation effect is applied in this theoretical investigation, where different electrode architectures are scrutinised subject to the predictions of the theory. The general formalism presented here is capable of describing previously constructed electroactuators [21–38], but we do not adjust the theory to exactly those architectures here. Instead, the simplest cases are investigated first.

In the present work, microstructured composites are explored, which create volumetric stress over a substantial proportion of the device to amplify the electroactuation effect. Highly porous, volume-filling electrodes in which pores are impregnated with Nafion<sup>®</sup>-type ionomer, as depicted in figure 2, can achieve the desired result. In such systems, double layers form at the pore walls across a large fraction of the thickness. Especially, if the pores are sufficiently narrow and dense, cation redistribution causes severe volumetric stress in a major proportion of the electrolyte phase. A description of the dynamic response of this type of device

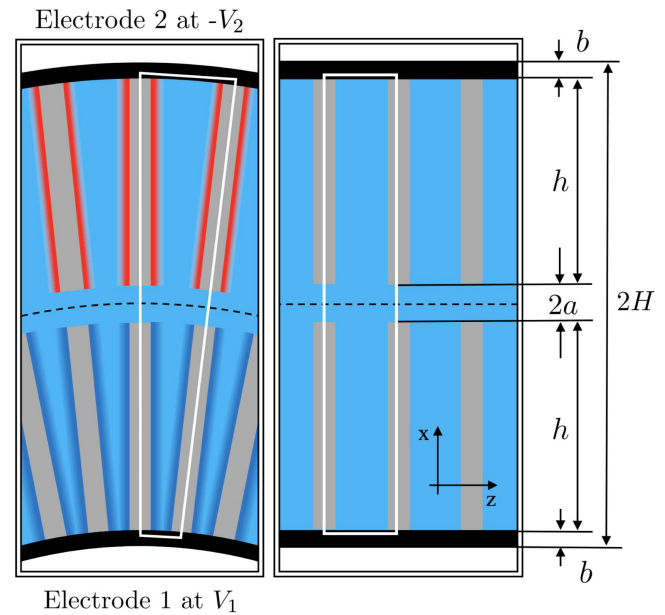


**Figure 2.** Microstructured polymer–electrolyte actuator curving in response to an applied voltage. Volume-filling electrodes (grey), of length  $h$ , are impregnated with a polymer–electrolyte (light blue for bulk). Electrochemical double layers (red and blue for illustrative effect) form along the entire pore wall. Between the two electrodes there is polymer–electrolyte membrane, of thickness  $2a$ , to ensure the electrodes do not short and facilitate ion transport. The remaining part of the electrode and casing, of length  $b$ , has been shown with solid black lines. The white rectangle/trapezium illustrates the ‘unit cell’ introduced to simplify the free energy of such systems. The dashed black line denotes the neutral line.

requires ‘transmission line charging’ theory [39–41]. In such systems, the length of the microstructured domains must be restricted if the electroactuator is to reach equilibrium within a reasonable time frame, say 1 s.

Since publication of [9] a significant amount of research has gone into understanding IPMCs with flat electrodes [2–8, 10–13]. This was, in part, because of the physically motivated theory formulated to understand the actuation mechanism. A natural development of IPMCs was to increase the surface area of the electrodes, so that more charge can accumulate upon application of a voltage, and therefore, increase the resulting curvature. The devices that have been constructed with high surface area electrodes were generally modelled through the assumption that the strain/stress was directly proportional to the accumulated charge [30–34, 36, 37]. This permitted fitting of experimental data to find the constant of proportionality, but did not lead to quantitative predictions and a physical understanding of these greatly improved devices. In terms of conceptual theoretical framework, there has been no equivalent to [9], as far as the authors are aware, for high surface area IPMCs. This has motivated the development of the theory presented in this article. It strives to describe, using an analytical formalism, the relationship between curvature and applied voltage, and its time dependence, with all relevant system parameters accounted for in

order to understand how higher surface area electrodes can improve the electroactuation effect.

Subsequently, the structure of the investigated microstructured composites will be presented. The simplifying assumptions are then outlined before the basic equations are derived from the general free energy functional. Equilibrium curvature is then calculated as a function of the applied voltage and the factors that can increase the actuator strength are analysed. The dynamics of approaching the equilibrium curvature upon application of a voltage step is then discussed. Finally, we investigate the actuator under load. Due to a large number of parameters and variables, all defined in the text, the list of symbols are also presented in table 1.

## 2. Microstructured composite model

In an IPMC, the electrode is metallic and the ionic polymer is a material like a Nafion<sup>®</sup>-ionomer with one large mobile cation [9–12]. Generally, the principle that is applied here to improve IPMCs, as done many times before [21–38], is to increase the proportion of the device that causes volumetric stress. Here two types of microstructured IPMCs are studied, both of which can be seen in figures 2 and 3.

On the left hand side of figure 3, a microstructured composite with cylindrical pores is shown. The system consists of long, cylindrical domains in the electrodes, of radius  $r_c$ , which are much larger than the double layer thickness. The induced volumetric stress in cylindrical pores will tend to bend the actuator in 2D, owing to the symmetry of the pore. For the electroactuator to bend in 1D it must be constrained. Here, when the IPMC curves, the cylindrical pores are assumed to deform ideally into elliptical pores. A symmetrical configuration of cylindrical domains on each side of the neutral line in the relaxed state is also considered. This permits the concept of a unit cell to be introduced, as illustrated in figures 2 and 3, which greatly simplifies the calculation of the free energy.

The second structure that we investigate consists of electrodes with slits filled with polymer–electrolyte, as seen in the right hand side of figure 3. These slits run along the width of the IPMC. This electrode architecture will also naturally bend in 2D, but we only consider 1D bending here. Again, a symmetrical configuration of slits on either side of the neutral line is adopted so that a unit cell concept can be utilised.

## 3. Simplifying assumptions

The phase-separated, nanoporous structure of the embedded ionomer phase is not explicitly accounted. The ionomer phase is considered as a uniform, volume-filling porous medium for expansion, with a constant number of spatially fixed charges which are balanced by the water-dissolved counterions. The ionomer phase appears in the mathematical formalism

**Table 1.** (i) Typical values, as reported in [10, 16]. (ii) The parameters displayed here are the investigated ones, based on experimentally attainable values [42, 43]. (iii) Both the bulk and Young's moduli are effective parameters, which need to be estimated for the specific composition and structure of the device. The range of values stated here encompasses values for materials used in ionomeric actuators [9–12, 20]. Since the ratio of bulk modulus to Young's modulus only appears in the dimensionless actuator constant, the estimate made for its value becomes somewhat insensitive to how the effective parameter is calculated. Both the rule of mixtures and effective medium theory give  $K/E \sim 2$  for a composite containing roughly equal volumes of metal and ionomer. (iv) These parameters appeared in previous works [10, 11] and the values here should be the same since they only depend on the polymer–electrolyte. The relative permittivity,  $\epsilon$ , was estimated to be 10 from effective medium theory [10]. (v) The differential capacitance was calculated using the Debye length and a voltage drop of 1 V across the double layer [19]. Values of ionic conductivity for bulky cations in an ionomer were taken from [2, 44, 45]. (vi) In the equations of this work,  $\tau_c$  and  $\tau_s$ , the characteristic diffusion time for the cylindrical and slit structure, respectively, appear, not  $\tau$ . (vii) Characteristic time of mechanical response depends on the length and thickness of the actuator, as well as the effective Young's modulus [46, 47]. (viii) Typical voltage window [10, 16]. Dimensionless voltage is equal to the electrostatic potential drop across the double layer divided by thermal voltage,  $k_B T/e$ .

Symbols, parameters, typical values		
Symbol	Name	Typical Value
$L_0$	Macroscopic length	1–3 cm <sup>(i)</sup>
$W_0$	Macroscopic width	0.5–1 cm <sup>(i)</sup>
$S_0$	Macroscopic surface area of beam	0.5–3 cm <sup>2</sup> <sup>(i)</sup>
$H$	Device half thickness	75–150 $\mu\text{m}$ <sup>(ii)</sup>
$a$	Half thickness of separating membrane	10–40 $\mu\text{m}$ <sup>(ii)</sup>
$h$	Microstructured electrode thickness	20–80 $\mu\text{m}$ <sup>(ii)</sup>
$b$	Remaining device casing thickness	10–40 $\mu\text{m}$ <sup>(ii)</sup>
$r_u$	Radius of porous unit cell	0.2–2 $\mu\text{m}$ <sup>(ii)</sup>
$l_u$	Width of slit unit cell	0.4–4 $\mu\text{m}$ <sup>(ii)</sup>
$r_c$	Cylindrical pore radius	0.1–1 $\mu\text{m}$ <sup>(ii)</sup>
$l_s$	Slit pore width	0.2–2 $\mu\text{m}$ <sup>(ii)</sup>
$E$	Young's modulus	$\sim 0.1$ –100 GPa <sup>(iii)</sup>
$K$	Bulk modulus	$\sim 1$ –100 GPa <sup>(iii)</sup>
$v$	Elemental excess volume	0.1–1 nm <sup>3</sup> <sup>(iv)</sup>
$l_B$	Bjerrum length	5–10 nm <sup>(iv)</sup>
$\lambda_D$	Debye length	1–5 Å <sup>(iv)</sup>
$\gamma$	Compacity	0.1–0.5 <sup>(iv)</sup>
$\epsilon$	Relative permittivity	10 <sup>(iv)</sup>
$C$	Capacitance	10 $\mu\text{F cm}^{-2}$ <sup>(iv)</sup>
$\Sigma$	Ionic conductance	$\sim 5 \times 10^{-3}$ S m <sup>-1</sup> <sup>(v)</sup>
$\tau$	Characteristic time of diffusion charging	0.1 $\mu\text{s}$ <sup>(vi)</sup>
$\tilde{\tau}$	Characteristic time of transmission line	$\sim 0.1$ s <sup>(vi)</sup>
$\tau_M$	Characteristic time of mechanical response	$\sim 10$ –100 ms <sup>(vii)</sup>
$\psi$	Voltage drop across double layer	$ \psi  < 2$ V <sup>(viii)</sup>
$V$	Dimensionless applied voltage	$ V  < 80$ <sup>(viii)</sup>

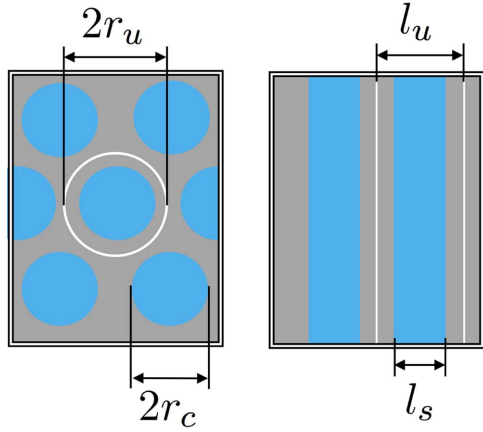


**Figure 3.** The two microstructured electrode architectures of IPMCs investigated here, depicted in the relaxed state. The porous cylindrical electrode architecture on the left is described by two key parameters: the radius of the unit cell,  $r_u$ , and the radius of the cylindrical pore,  $r_c$ . The microstructured IPMC on the right with slit electrodes filled with polymer–electrolyte membrane has the width of the unit cell,  $l_u$ , and the width of the polymer–electrolyte slit,  $l_s$ , as parameters. The characteristic perimeter for microstructured electrodes with slits is  $2W_0$ , which is twice the width of the actuator. Cylindrical pores and slits are orientated normal to the surface of the beam, as depicted in figure 2.

through elastic and electrostatic free energy contributions of the actuator.

The ionomer phase domains in the electrode are considered to be straight and monodisperse. This is generally an idealization, but extension to more complicated structures would pose no problem, provided the double layer thickness is shorter than any characteristic curvature/roughness dimensions [48, 49].

Only bending in 1D is described here. It is also assumed that the gradients of deflection are small and linear elasticity theory remains valid. The considered actuator architectures, however, turn out to be so responsive to applied voltage that this assumption only applies for the lower bounds of the estimated parameters and applied voltages. For the upper bounds of the estimates, the obtained curvature indicates that the actuator should form a spiral, which cannot be described with the presented theory. Hence, the figures only display examples that are within the bounds of the theory.

Reverse actuation produces a voltage orders of magnitude smaller than that applied to generate the same curvature [6–9, 51–55]. Thus, the responses from applied voltage and external forces are essentially decoupled, and the two can be summed together to afford the net deflection.

#### 4. Basic equations

Under the given assumptions, an approximate, general form of the free energy functional reads

$$\mathcal{F}[\psi] = \frac{1}{3}ES_0H^3\kappa^2 + \int_V d\mathbf{r} \left[ -\frac{\epsilon}{8\pi}(\nabla\psi(\mathbf{r}))^2 + e\rho(\mathbf{r})\psi(\mathbf{r}) + k_B Tg(\mathbf{r}) - K\nu\kappa\rho(\mathbf{r})x \right], \quad (1)$$

in the absence of external forces and when bending only occurs in 1D, with constant curvature,  $\kappa$ . The first term describes the elastic energy, where  $E$ ,  $H$  and  $S_0$  are the effective Young's modulus, half thickness of electroactuator (see figure 2 for explanation) and macroscopic external surface area of the bending face, respectively. The Young's modulus is an effective parameter of the theory because of the interpenetrating domains of electrode and ionomer (an estimate was obtained with the rule of mixtures and effective medium theory, as reported in table 1). Term two is the self energy of the electrostatic potential,  $\psi(\mathbf{r})$ . Term three is the electrostatic energy of ions, related to the excess charge concentration  $\rho(\mathbf{r}) = c_+(\mathbf{r}) - c_-(\mathbf{r})$ , where  $c_+(\mathbf{r})$  and  $c_-(\mathbf{r})$  are the density of cations and anions, respectively. In equation (1)  $\epsilon$  and  $e$  are relative permittivity and elementary charge, respectively. The fourth term is the lattice-gas entropic term associated with ions, where  $k_B$  and  $T$  are Boltzmann's constant and temperature, respectively. In the last term, the mechanical and electrostatic energy are coupled through curvature, which depends, in part, on the excess charge concentration [9–12]. It is assumed that ions in the double layer play the role of volumetric defects in the homogenous elastic medium. The energy contribution from the volumetric defects in the double layer is motivated from the misfitting sphere model [50]. For the case of one mobile ion, the stress induced by the corresponding volumetric defect is taken to be  $K\nu$ , where  $K$  and  $\nu$  are the effective bulk modulus (see table 1 for more details) and elemental volume associated with each cation, respectively [10, 11].

Minimising the free energy functional with respect to  $\psi$

$$\frac{\delta\mathcal{F}}{\delta\psi} = 0 \quad (2)$$

gives the Poisson equation

$$\nabla^2\psi(\mathbf{r}) = -\frac{4\pi e}{\epsilon}\rho(\mathbf{r}). \quad (3)$$

The simplest form of the lattice-gas energy for the case with the single mobile ionic species, cations in our case, is

$$g(\mathbf{r}) = c_+(\mathbf{r})\ln\left\{\frac{c_+(\mathbf{r})}{c_{\max}}\right\} + (c_{\max} - c_+(\mathbf{r}))\ln\left\{1 - \frac{c_+(\mathbf{r})}{c_{\max}}\right\}, \quad (4)$$

expressed through their concentration,  $c_+(\mathbf{r})$ , and the maximal concentration of cations,  $c_{\max}$  [10, 11, 19].

Minimisation of the free energy functional with respect to the cation concentration gives the electrochemical potential

$$\bar{\mu}_+ = e\psi(\mathbf{r}) - K\nu\kappa x + k_B T \ln\left\{\frac{c_+(\mathbf{r})}{c_{\max} - c_+(\mathbf{r})}\right\}. \quad (5)$$

Equating the electrochemical potential of the cations with their chemical potential in the neutral plane (see figure 3), thus satisfying chemical equilibrium, obtains

$$c_+(\mathbf{r}) = \frac{c_{\max}}{\left[\frac{c_{\max}}{c_0}(1 + \kappa x) - 1\right] \exp\left\{\frac{e\psi(\mathbf{r}) - K\nu\kappa x}{k_B T}\right\} + 1}. \quad (6)$$

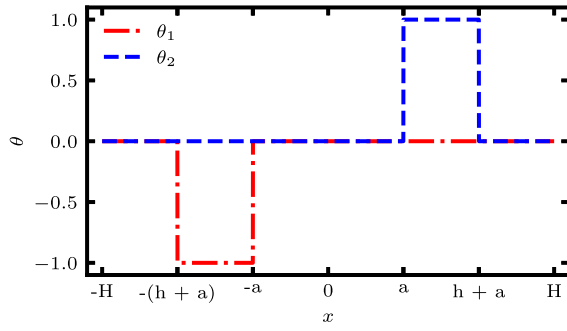


Figure 4. Graphical representation of the  $\theta_i(x)$  function.

The concentration of cations in the bulk is the same as that of anions. If the number of anionic species are fixed in each infinitesimal element with thickness  $dx$ , their concentration dependence goes as

$$c_-(x) = \frac{c_0}{1 + \kappa x}. \quad (7)$$

One then arrives at the investigated form of the Poisson equation

$$\nabla^2 \psi(\mathbf{r}) = \frac{4\pi e c_0}{\epsilon(1 + \kappa x)} \times \frac{\left[1 - \frac{\gamma}{1 + \kappa x}\right] \left[\exp\left\{\frac{e\psi(\mathbf{r}) - K_V \kappa x}{k_B T}\right\} - 1\right]}{\left[1 - \frac{\gamma}{1 + \kappa x}\right] \exp\left\{\frac{e\psi(\mathbf{r}) - K_V \kappa x}{k_B T}\right\} + \frac{\gamma}{1 + \kappa x}}. \quad (8)$$

This is not amenable to analytical solution, however. To progress further, we employ the assumption of  $1 \gg \kappa x$ , and drop all dependence of equation (8) on  $\kappa$ . It is then simple to obtain the first integral, which can be used to find the charge accumulated in the double layer [19].

To find the relation between the curvature and voltage, it is prudent to introduce the unit cell concept. The free energy can be written as the sum of the elastic energy of bending, i.e. the first term in equation (1), plus the remaining free energy contributions in equation (1) for a unit cell multiplied by the number of unit cells. In the supplementary information (SI), available online at [stacks.iop.org/SMS/27/075056/mmedia](http://stacks.iop.org/SMS/27/075056/mmedia), the free energy of one unit cell, for the two types of micro-structured electrodes, is studied with different levels of approximation. In the ‘first order’ solution, we account for the contribution to bending only from volumetric stress [10], while the term that couples the curvature to the electrostatic pressure is neglected. In the ‘second order’ solution (provided in the SI), the contribution from electrostatic pressure is included as well as from the volumetric stress [11].

The free energy function due to curvature dependent terms,  $\mathcal{F}_\kappa$ , for the ‘first order’ solution can be written as

$$\mathcal{F}_\kappa = \frac{1}{3} E S_0 H^3 \kappa^2 - NP \frac{K_V \kappa}{4\pi l_B \lambda_D} \int_{-H}^H x \sum_{i=1,2} \sigma_i(V_i) \theta_i(x) dx. \quad (9)$$

In figure 4,  $\theta_i(x)$  is graphically presented. To get to equation (9), we have integrated the charge density over the double layer to obtain the net charge accumulated there. The

equilibrium curvature is determined by the minimum of the free energy, equation (9), which depends on the interplay between the two terms shown.

One of the central parameters of this theory is device thickness,  $2H$ , as outlined in figure 2. The elastic energy penalty of curving is strongly dependent on it; thinner IPMCs have larger curvature because the elastic energy penalty is smaller. However, the device thickness is also a key parameter in the dynamics and the work such devices are capable of performing, and so reducing device thickness is not always favourable.

The number of unit cells,  $N$ , and a characteristic perimeter of a unit cell,  $P$ . Generally, increasing the density of unit cells and its characteristic perimeter enhances electroactuation, since the net charge accumulated scales with the surface area. Here, the surface charge density,  $e\sigma_i(V_i)/4\pi l_B \lambda_D$ , and areas of electrodes have been explicitly included to reveal how actuation depends on system parameters. For electrodes with cylindrical ionomer-filled domains, the number of unit cells is  $S_0/\pi r_u^2$  and the characteristic dimension  $2\pi r_c$ , as seen in figure 3; for the slit composite these parameters are  $L_0/l_u$  and  $2W_0$ , respectively, where  $L_0$  and  $W_0$  are the device length and width.

## 5. Results and discussion

### 5.1. Equilibrium curvature–voltage dependence

Minimising equation (9) with respect to curvature, integrating over the thickness and using the solution for surface charge density (see SI, and [10, 19] for details) gives an equation for the equilibrium dimensionless curvature,  $\mathcal{K} = \kappa H$ , as a function of applied voltage

$$\mathcal{K} = \alpha_M \sum_{i=1,2} \sqrt{2 \left[ \pm V_i + \frac{1}{\gamma} \ln \{1 - \gamma + \gamma \exp\{\mp V_i\}\} \right]}. \quad (10)$$

Voltage drops across double layers of electrode 1 and 2,  $V_1$  and  $-V_2$ , respectively, appear in units of thermal voltage,  $k_B T/e$ . In the presented sign convention, the positive sign of the first voltage term is associated with electrode 1. In an experiment one does not control the voltage drop across each double layer separately, but the overall voltage drop across both electrodes,  $V = V_1 + V_2$  ( $V_1$  and  $V_2$  are positively defined). Therefore, curvature must be expressed in terms of the total voltage drop across the electrodes. The applied voltage is distributed between the two electrodes depending on the the ratio of average concentration of cations,  $c_0$ , over maximal concentration,  $c_{\max}$ ; seen in equation (10) through compacity,  $\gamma = c_0/c_{\max}$  [10, 11, 19]. A relation for  $V_1$  in terms of  $V$  reads [10, 11]

$$V_1 = \ln \left\{ \left( \frac{\gamma}{1 - \gamma} \right) \frac{\exp\{(1 - \gamma)V\} - 1}{1 - \exp\{-\gamma V\}} \right\}, \quad (11)$$

and since  $V_2$  is a function of  $V$  and  $V_1$ , the voltage drop across the cationic rich Nafion<sup>®</sup> membrane can also be determined.

**Table 2.** (i) Microstructured dimensionless actuator constants were determined from table 1. Specifically, the values taken were:  $K/E \approx 2$ ;  $2r_c = l_c = 200 \text{ nm} - 2 \text{ } \mu\text{m}$ ;  $2r_u = l_u = 400 \text{ nm} - 4 \text{ } \mu\text{m}$ ;  $\xi = 0.96 - 0.5$ ;  $l_B = 5 \text{ nm}$ ;  $\lambda_D = 2 \text{ } \text{Å}$ ;  $v = 0.1 - 1 \text{ nm}^3$ . The range of values come from the different values of the stated parameters in the previous sentence. (ii) Values of the flat IPMC dimensionless actuator constant were taken from [10].

Dimensionless actuator constants and typical values		
Type of electrode	Dimensionless actuator constant	Range of values
Microstructured	$\alpha_M = \frac{3 K NP\xi}{2 E 2S_0} \frac{v}{4\pi l_B \lambda_D}$	$\sim 10^{-3} - 10^{-6}$ (i)
Cylindrical pores	$\alpha_c = \frac{3 K \rho_c r_c \xi v}{8 E l_B \lambda_D} \equiv \frac{3 K P_c \xi}{8\pi E r_c} \frac{v}{l_B \lambda_D}$	$\sim 10^{-3} - 10^{-6}$ (i)
Slit pores	$\alpha_s = \frac{3 K \rho_s \xi v}{8\pi E l_B \lambda_D} \equiv \frac{3 K P_s \xi}{8\pi E l_s} \frac{v}{l_B \lambda_D}$	$\sim 10^{-3} - 10^{-6}$ (i)
Flat	$\alpha_F = \frac{3 K \lambda_D S}{2 E H S_0} c_0 v \equiv \frac{3 K S}{4\sqrt{\pi} E S_0} \frac{v}{H} \frac{c_0^{1/2}}{l_B^{1/2}}$	$\sim 10^{-5} - 10^{-6}$ (ii)

The dimensionless actuator constant of microstructured electrodes is given by

$$\alpha_M = \frac{3 K NP\xi}{2 E 2S_0} \frac{v}{4\pi l_B \lambda_D}, \quad (12)$$

which determines the ‘strength’ of actuation. Along with device thickness, the dimensionless actuator constant is one of the key parameters of the theory. The value of  $\alpha_M$  increases with  $K/E$ , owing to the decreasing relative cost of elastic energy from bending [10, 11]. Here,  $\xi = h(h + 2a)/H^2$  shall be referred to as the electrode utilisation factor. It characterises the extent of the presence of the electrode and membrane in the whole construction. The geometric factor of microstructured electrodes,  $NP\xi/2S_0$ , has little resemblance to that of flat electrodes,  $S/S_0H$  [10, 11]. Since the electro-actuator thickness only appears through  $\xi$  in the dimensionless actuator constant for volume-filling electrodes, the dependence on  $H$  has been suppressed.

In the dimensional version of equation (10),  $H$  appears in the denominator on the rhs, demonstrating that as the thickness increases, the resulting curvature decreases due to the elastic energy penalty. Increasing the surface area of the electrodes, for a given thickness, results in larger curvatures for volume-filling electrodes [21–38]. Such an enhancement could be implemented by increasing the density of pores, for example.

As the concentration of ions increases, the Debye length,  $\lambda_D$ , decreases, which results in larger  $\alpha_M$ . This is due to enhanced capacity of the pore to admit charge for a given voltage. Increasing the concentration of cations, however, can also increase  $\gamma$ , which inhibits the enhancement from  $\alpha_M$ . Both of these dependences go with the square root of concentration (see interpolation formula, namely equation (13)), which results in partial cancellation of the dependence on concentration.

For this volumetric mechanism, equation (12) actually remains valid for any shape of the pore as long as its characteristic perimeter is much longer than the Debye length [48, 49]. In table 2 (see also table 3, where definitions of parameters for the studied electrode architectures are stated),

**Table 3.** Parameters for studied architectures.

Parameter	Name	Form
$N_c$	Number of cylindrical pores	$S_0/\pi r_u^2$
$N_s$	Number of slits	$L_0/l_u$
$P_c$	Perimeter of pore	$2\pi r_c$
$P_s$	Perimeter of slit	$2W_0$
$\rho_c$	Density of cylindrical pores	$S_0/\pi r_u^2$
$\rho_s$	Density of slits	$1/l_u$
$p_c$	Porosity of cylindrical pores	$r_c^2/r_u^2$
$p_s$	Porosity of slits	$l_s/l_u$
$\xi$	Electrode utilisation factor	$h(h + 2a)/H^2$

the dimensionless actuator constants for the two types of microstructured electrodes studied here are stated, and for reference the actuator constant of flat electrodes has been reproduced [10, 11]. For the typical values of parameters in table 1, a range of possible values for the actuator constants are also displayed. It is evident that the actuator constants for microporous electrodes [21–38] can potentially be orders of magnitude larger than that of flat electrodes [2–13]. Therefore, by changing the internal electrode architecture, the response of the electroactuator can be greatly enhanced. Thus, microstructured composites should be capable of performing orders of magnitude more work, for the same applied voltage, than similar IPMCs with flat electrodes (for estimates see the last section of the paper).

For microstructured electrodes, there are two ways of expressing the dimensionless actuator constant: through the density of pores,  $\rho$ , or porosity,  $p$ . The surface density for cylindrical pores is  $1/\pi r_u^2$  and linear density for slit pores  $1/l_u$ . It is clear that increasing the density of ‘unit cells’ increases electroactuation, due to the correspondingly larger volumetric stress. The porosity of cylindrical pores is given by  $r_c^2/r_u^2$  and porosity of the slit architecture  $l_s/l_u$ . Increasing porosity corresponds to utilising a large volume fraction of the device for the polymer–electrolyte membrane, which aids through increasing the net charge accumulated. It is evident that smaller pores, for a given porosity, leads to larger actuator constants.

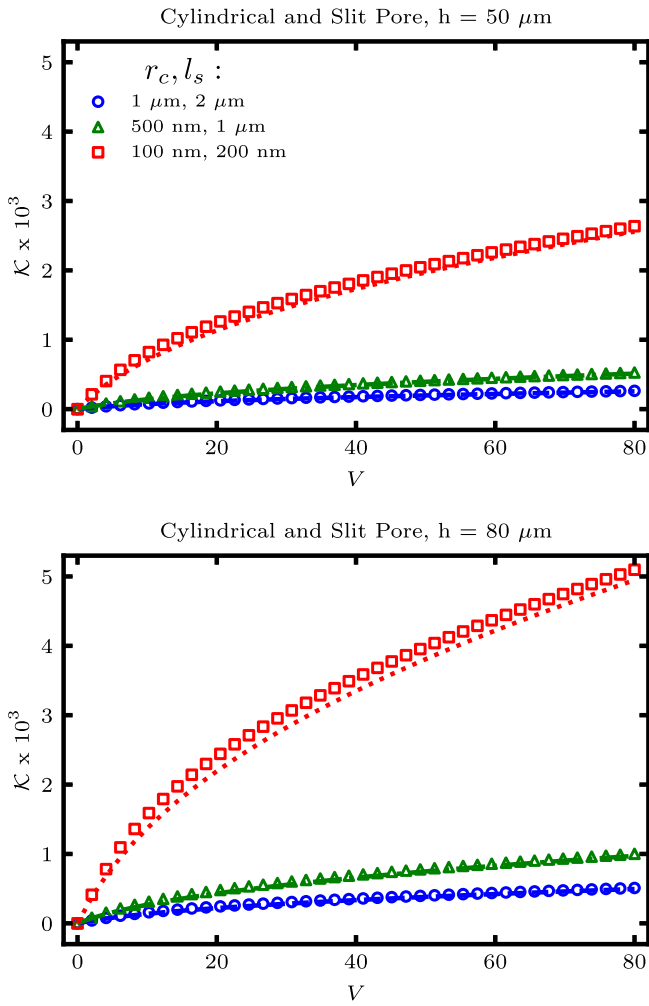


**Figure 5.** Full numerical solution, seen by symbols, and interpolation formula, displayed with lines, have satisfactory agreement to justify the use of the interpolation formula. Both architectures, cylindrical pores and slits, fall onto the same curve for the studied parameters. Dimensionless curvature, for the cylindrical and slit pore, as a function of dimensionless voltage for the indicated pore radius,  $r_c$ , or width,  $l_s$ , and  $h$ ; while in all cases  $\gamma = 0.5$  [11],  $K/E = 2$ ,  $H = 100 \mu\text{m}$ ,  $r_u = 2r_c$ ,  $l_u = 2l_s$ ,  $a = b$ ,  $v = 0.5 \text{ nm}^3$ ,  $\mu_B = 5 \text{ nm}$ ,  $\lambda_D = 2 \text{ \AA}$ .

At linear response,  $V \ll 1$ , equations (10) and (11) can be expanded in powers of  $V$  to find  $\mathcal{K} = \alpha_M \sqrt{1 - \gamma} V$ . In the limit of large voltages,  $V \gg 1$ , equations (10) and (11) simplify to  $\mathcal{K} = \alpha_M \sqrt{8(1 - \gamma)} V$ . These two limiting equations can be combined into an interpolation formula

$$\mathcal{K} = \alpha_M \frac{\sqrt{1 - \gamma} V}{\sqrt{1 + \frac{V}{8}}}. \quad (13)$$

The voltage dependent factor of which is identical to that of [10], but the actuation parameter,  $\alpha_M$ , is significantly larger here and depends differently on system parameters. Figure 5 shows that the full numerical solution, given by equations (10) and (11), agrees remarkably well with the interpolation formula, equation (13). Subsequently, equation (13) will be used.

For the actuator to ‘bend back’, there must be a component of the Maxwell stress in the considered direction of bending [11]. The ‘second order’ solution for cylindrical microstructured electrodes is different from the ‘first order’ one, but for the slit electrode structure there is no significant difference. Hence, we found that cylindrical microstructured electrodes can potentially bend backwards if  $\gamma < 1/2$  [11]. This is an advantage of employing slit microstructured electrodes over the cylindrical architecture. The derivation for the ‘second order’ solution for the cylindrical electrodes, as shown in the SI, follows that in [11]. We obtain for the curvature–voltage dependence for the ‘second order’ solution for cylindrical electrodes

$$\mathcal{K} = \alpha_c \frac{\sqrt{1 - \gamma} V}{\sqrt{1 + \frac{V}{8}}} + \frac{1}{3} \beta_c (1 - 2\gamma) \sqrt{2(1 - \gamma)} V^{3/2}, \quad (14)$$

where

$$\beta_c = \frac{3}{8} \frac{\rho_c r_c \xi}{E} \frac{k_B T}{l_B \lambda_D}. \quad (15)$$

The voltage dependence does not differ in form from [11], but the expressions for the electroactuator constants,  $\alpha_c$  and  $\beta_c$ , through physical and geometrical parameters of the system, are principally different, and the typical numerical values for them can be orders of magnitude larger for microstructured electrodes. It is interesting to note that  $\alpha_c/\beta_c = Kv/k_B T$  is the same as that of flat electrodes [11]. In figure S1 of the SI, the curvature–voltage dependence of equation (14) is displayed.

## 5.2. Dynamic response

If the characteristic time scale of elastic deformation of the beam is much longer than the time required to redistribute ions, once the bias voltage is applied, the beam will bend to mechanical equilibrium following its mechanical response. On the other hand, IPMCs with long pores that have a time scale of ion redistribution,  $\tilde{\tau}$ , defined below and in table 1, which exceeds the time scale of the mechanical response,  $\tau_M$  [46, 56]. In fact, extended microstructured domains are of interest, to enhance the ‘strength’, but not so long that the time taken to reach equilibrium is over 1 s [57]; this constraint imposes an upper limit on the length of pores.

Upon application of a voltage step, the pores in the electroactuator are not charged momentarily, but subject to the response ability of a linear ‘transmission line’ [39–41]. The dynamics of the beam at  $t < \tau_M$  depends on the mechanical response, while at  $t > \tau_M$  the dynamics of curvature follows transmission line theory. Since  $\tilde{\tau} \gg \tau_M$ , the response at small time does not influence the overall dynamics significantly. For the description of the dynamical response, the double layer capacitance is taken at its final, constant value.

In the studied microstructured composites, there is not one microstructured electrode in equilibrium with a large reservoir of electrolyte, as is usually the case [39, 40], but a tandem electrode structure, as seen in figure 2. Between the two electrodes there is a separating polymer–electrolyte

membrane. If this part of the electroactuator is small, the contribution it makes to the net charge of each pore can essentially be neglected. Charge conservation then requires that the net charge of one microstructured electrode pore must be approximately equal and opposite to the other. The dynamics of a tandem transmission line is then approximated with the assumption that the characteristic times of charging of each microstructured electrode are equal. Generally this might not be the case, but a more sophisticated theory may be needed when dealing with practical systems.

In [39] transmission line charging (see also [40, 41]) of a long, cylindrical pore in the electrode was outlined. There, edge effects were neglected and capacitance was constant. Edge effects are also neglected here, but capacitance should not be constant. Furthermore, neglecting any influence of curvature on pore charging permits a dynamic equation for the surface charge density

$$\tilde{\sigma}_i(V_i, x, t) = \sigma_i(V_i)\theta_i(x)\phi(x, t), \quad (16)$$

given in dimensionless form here; where in the smallness of a

$$\begin{aligned} \phi(x, t) = & 1 - \frac{2}{\pi} \sum_{n=0}^{\infty} \frac{(-1)^n}{\left(n + \frac{1}{2}\right)} \cos\left[\left(n + \frac{1}{2}\right)\pi\left(1 - \frac{x}{h}\right)\right] \\ & \times \exp\left\{-\left(n + \frac{1}{2}\right)^2 \frac{t}{\tau_c} \left(\frac{\pi r_c}{2h}\right)^2\right\}, \end{aligned} \quad (17)$$

with  $\tau_c = Cr_c/2\Sigma$  in the cylindrical pore, where  $C$  and  $\Sigma$  are double layer capacitance per unit surface area of the electrode and ionic conductance, respectively [39]. Integration of charge density over the channel length gives the total charge in the pore. The characteristic time scale of pore charging does not remain the same throughout charging. At small times, the time evolution of pore charging has the characteristic time scale of  $\tau_c$ . While at long times, the characteristic charging time,  $\tilde{\tau}_c = 4\tau_c(2h/\pi r_c)^2$ , is significantly longer than at short times, since  $h \gg r_c$  [39].

The solution for the time dependence of dimensionless curvature,  $\mathcal{K}(t)$ , is obtained from minimising equation (9) with respect to  $\kappa$  and introducing the time dependent surface charge density

$$\mathcal{K}(t) = \frac{3K}{8E} \frac{\rho_c r_c v}{H^2 l_B \lambda_D} \int_{-H}^H \sum_{i=1,2} \tilde{\sigma}_i(V_i, x, t) x dx. \quad (18)$$

Integrating and noting the smallness of  $a$  gives

$$\begin{aligned} \mathcal{K}(t) = & \frac{32\alpha_c \sqrt{1-\gamma} V}{\pi^3} \sum_{n=0}^{\infty} \frac{(-1)^n}{\sqrt{1 + \frac{V}{8}} (2n+1)^3} \\ & \times \left[ 1 - \exp\left\{-(2n+1)^2 \frac{t}{\tilde{\tau}_c}\right\} \right]. \end{aligned} \quad (19)$$

Transmission line theory for slit electrodes can simply be described with swapping  $r_c$  for  $l_s$ ; the characteristic time is then referred to as  $\tilde{\tau}_s$  and is given by  $8h^2C/\pi^2 l_s \Sigma$ .

For longer, narrower microstructured pores in the electrodes the response time increases. The response times are quicker and curvatures larger for shorter pores, but the ability of the device to perform work also diminishes (see next

section). Applications of the discussed electroactuator require the work that can be performed to be optimised, rather than the fastest response time and largest curvature. In figure 6, example dependences of time dependent curvature on pore length have been displayed to demonstrate that the ionomer-filled domains cannot be much longer than  $50 \mu\text{m}$  if equilibrium curvature is to be reached within 1 s [57]. Such time responses could be required in applications where these electroactuators are mimicking/reproducing muscle movement in animals [16, 22, 51, 57].

At small times, beam dynamics is dictated by the mechanical response, not transmission line theory, so the limiting behaviour at small times is not investigated. At large times, the dynamics of curvature can be approximated by  $K(t) \approx K_{\chi(\infty)}(1 - \exp\{-t/\tilde{\tau}\})$ , which has been included in figure 6 to compare with the full solution, equation (19).

### 5.3. External load

Under an applied force the actuator will bend, inducing an output voltage. It has been demonstrated [6–9, 51–55], however, that reverse actuation results in voltages that are orders of magnitude smaller compared to the voltages applied to generate the same curvature as forward actuation. Therefore, as a first approximation, external mechanical forces can be decoupled from ion distributions in the ionomer. Therefore, according to the method of superposition [53], the deflection at each point is given by the sum of the deflection from electroactuation,  $w_E$ , and mechanical forces,  $w_M$ . Integrating the text-book equation for curvature, for small gradients of deflection, with one end of the actuator fixed gives

$$w_E = -\frac{\kappa y^2}{2}. \quad (20)$$

For a cantilever with an end-loaded, point-like mass,  $m$ , the displacement is given by

$$w_M = \frac{mgL_0^3}{6EI} \left[ 3\left(\frac{y}{L_0}\right)^2 - \left(\frac{y}{L_0}\right)^3 \right]; \quad (21)$$

where  $L_0$  and  $I$  are macroscopic length of the actuator and second moment of inertia, with the latter given by  $W_0 H^3/3$  [58]. Substituting both of these expressions, for the case of the slit architecture, into the linear superposition gives

$$w|_{L_0} = \frac{L_0^2}{EH} \left[ \frac{3}{16\pi} \frac{K\xi\rho_s v}{l_B \lambda_D} \frac{\sqrt{1-\gamma} V}{\sqrt{1+V/8}} - \frac{L_0 mg}{W_0 H^2} \right], \quad (22)$$

which has been plotted in figure 7 for reference. The equation states that ‘more flexible’ (smaller value of  $E$ ) electroactuators have larger deflections. This is the same for the deflection due to applied mechanical force and applied voltage. To produce the maximum deflection under load, the beam should be as ‘flexible’ as possible. One might have expected that stiffer electroactuators are better because they are more resistive to external force, but this is not so because a softer beam will respond stronger to applied voltage. Therefore, the actuator should preferably operate in the parameter space where the

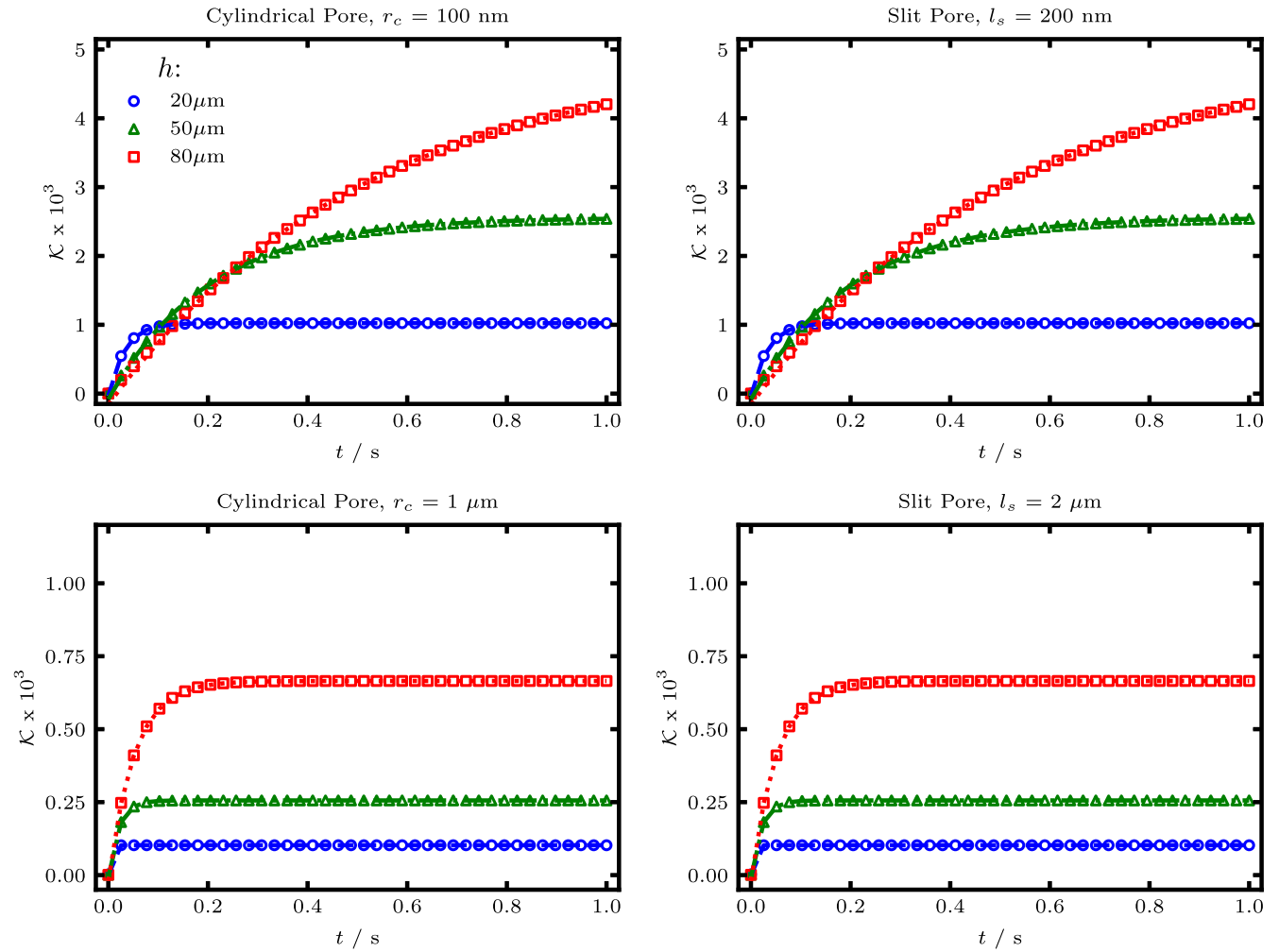


**Figure 6.** As the pore lengthens, the time taken to reach equilibrium curvature gets longer. Dimensionless curvature as a function of time for the indicated pore lengths and radii, for the following parameter values:  $C = 10 \mu\text{F cm}^{-2}$  [19];  $\Sigma = 5 \times 10^{-3} \text{ S m}^{-1}$  [2, 44, 45];  $V = 80$ ; see figure 5 for other parameters. Lines correspond to the approximate solution at large times and symbols to that of equation (19).

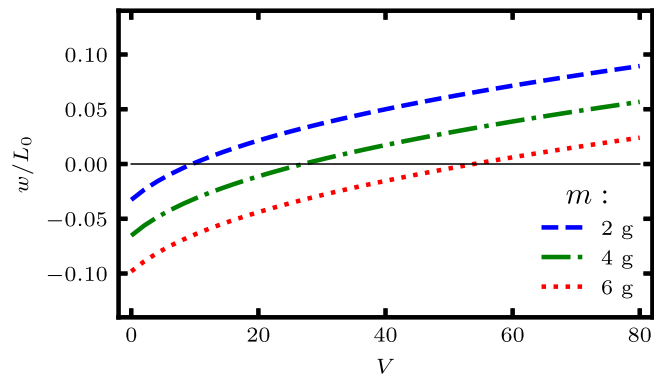


**Figure 7.** Larger masses require higher voltages to reach no net displacement. Tip displacement as a function of applied voltage and mass. Here  $K = 4 \text{ GPa}$ ,  $E = 8 \text{ GPa}$ ,  $L_0 = 1.5 \text{ cm}$ ,  $W_0 = 0.5 \text{ cm}$ ,  $H = 150 \mu\text{m}$ ,  $v = 1 \text{ nm}^3$ ,  $\xi = 0.96$ , and  $l_u = 0.4 \mu\text{m}$ .

voltage-induced force dominates, such that softer actuators enhance deflection.

Another interesting prediction is that, since the external mechanical force term depends more strongly on device thickness, a thicker electroactuator will resist external

mechanical forces more than the internal stresses created from double layer formation. Thus, a ‘stronger’ IPMC is one which is thicker (larger  $H$ ).

To highlight the improvement volume-filling electrodes offer over flat electrodes [21–38], we outline a simple equation to calculate the mass that microstructured IPMCs can hold and compare to flat electrode composites. The actuator itself is assumed to be light, so that when no voltage or mass is applied the actuator is resting in a horizontal, cantilever position. Consider an actuator that may sustain an end-loaded mass,  $m_{\text{max}}$ , for a given voltage, without changing the tip displacement. What is the mass for the maximal voltage,  $V_{\text{max}}$ ? This is given by the following formula

$$m_{\text{max}} = \frac{EW_0H^2\alpha_M \sqrt{1 - \gamma V_{\text{max}}}}{2gL_0 \sqrt{1 + \frac{V_{\text{max}}}{8}}}; \quad (23)$$

where  $g$  is the gravitational acceleration at the surface of the Earth. The mass an actuator can hold is directly proportional to the dimensionless actuator constant; this holds for both microstructured and flat IPMCs. Since the dimensionless actuator constant for microstructured composites can be

orders of magnitude larger than that of flat electrodes, microstructured IPMCs should be far superior to flat electrodes [21–38].

As previously mentioned, applications require the work IPMCs can conduct to be optimised, rather than the largest curvatures and smallest response times. As can be seen from equation (23), the mass electroactuators can hold scales with the square of device thickness. Therefore, thicker devices can sustain larger masses, but will respond more slowly and require larger voltages for the same curvature. The work these microstructured electroactuators can perform could be increased by constructing artificial muscles as bundles of electroactuators.

## 6. Conclusion

Here a theory for polymer–electrolyte electroactuators with volume-filling electrodes was developed. It was found that curvature, for the same device thickness and applied voltage, is significantly enhanced, potentially orders of magnitude, in comparison to flat electrodes. This result is in agreement with a large body of literature, as cited throughout the article. The actuator response time, which should be no longer than 1 s for applications, imposes an upper constraint on the pore length and thus actuator thickness. Results suggest that a complex device consisting of bundled elementary electroactuators could perform significant amounts of work in possible applications mentioned in the main text. The simple, analytical theory presented in this article is expected to stimulate further experimental and theoretical work on the various impacts of geometric and operational parameters.

## Acknowledgments

ZG was supported through the Junior Research Fellowship of the Thomas Young Center UK and a studentship in the Centre for Doctoral Training on Theory and Simulation of Materials at Imperial College London funded by the EPSRC (EP/L015579/1). ME acknowledges financial support of the Discovery Grants Program of the Natural Sciences and Engineering Research Council of Canada. HL acknowledges support from the Deutsche Forschungsgemeinschaft (Grant LO418/19-1). AAK thanks Alexander von Humboldt Foundation that supported his post-Senior-Humboldt-Award visit to the Institute of Theoretical Physics of the Heinrich-Heine University (HHU). The core part of this collaborative project was performed during the stay of ZG, AK and ME at the HHU Institute of Theoretical Physics, and all three are thankful to HL for hospitality.

## ORCID iDs

Zachary A H Goodwin  <https://orcid.org/0000-0003-2760-4499>

Michael Eikerling  <https://orcid.org/0000-0002-0764-8948>

Hartmut Löwen  <https://orcid.org/0000-0001-5376-8062>

Alexei A Kornyshev  <https://orcid.org/0000-0002-3157-8791>

## References

- [1] Oguro K, Asaka K and Takenaka H 1993 *Proc. 4th Int. Symp. on Micro Machine and Human Science (Nagoya, Japan)* pp 39–40
- [2] Lin J, Liu Y and Zhang Q 2011 *Polymer* **52** 540–6
- [3] Farinholt K M and Leo D J 2007 *J. Intell. Mater. Syst. Struct.* **18** 677–92
- [4] Nemat-Nasser S, Zamani S and Tor Y 2006 *J. Appl. Phys.* **99** 104902
- [5] Schicker D and Wallmersperger T 2013 *J. Appl. Phys.* **114** 163709
- [6] Aureli M, Prince C, Porfiri M and Peterson S D 2010 *Smart Mater. Struct.* **19** 015003
- [7] Cha Y and Porfiri M 2014 *J. Mech. Phys. Solids* **71** 156–78
- [8] Arumugam J, Srinivasa A and Reddy J 2013 *Compos. Struct.* **106** 461–9
- [9] Nemat-Nasser S and Li J Y 2000 *J. Appl. Phys.* **87** 3321–31
- [10] Lee A A, Colby R H and Kornyshev A A 2013 *J. Phys.: Condens. Matter* **25** 082203
- [11] Lee A A, Colby R H and Kornyshev A A 2013 *Soft Matter* **9** 3767–76
- [12] Wallmersperger T, Horstmann A, Kröplin B and Leo D J 2009 *J. Intell. Mater. Syst. Struct.* **20** 741–50
- [13] Nemat-Nasser S 2002 *J. Appl. Phys.* **92** 2899–915
- [14] Mirfakhrai T, Madden J D W and Baughman R H 2007 *Mater. Today* **10** 30–8
- [15] Hines L, Petersen K, Lum G Z and Sitti M 2017 *Adv. Mater.* **29** 1603483
- [16] Yu M, He Q, Yu D, Zhang X, Ji A, Zhang H, Guo C and Dai Z 2012 *Appl. Phys. Lett.* **101** 163701
- [17] He Q, Yu M, Yu D, Ding Y and Dai Z 2013 *J. Bionic Eng.* **10** 329–67
- [18] He Q, Yang X, Wang Z, Zhao J, Yu M, Hu Z and Dai Z 2017 *J. Bionic Eng.* **14** 567–78
- [19] Kornyshev A A and Vorotyntsev M A 1981 *Electrochem. Acta* **26** 303–23
- [20] Jo C, Pugal D, Oh I-K, Kim K J and Asaka K 2013 *Prog. Polym. Sci.* **38** 1037–66
- [21] Luo Y and Yu X 2016 *Eur. Polym. J.* **82** 290–9
- [22] Kong L and Chen W 2014 *Adv. Mater.* **26** 1025–43
- [23] Baughman R H et al 1999 *Science* **284** 1340–4
- [24] Kosidlo U, Micusík M O M, Ćirić-Marjanović G, Randriamahazaka H, Wallmersperger T, Aabloo A, Kolaric I and Bauernhansl T 2013 *Soft Matter Struct.* **22** 104022
- [25] Liu S, Liu Y, Cebeci H, de Villoria R G, Lin J-H, Wardle B L and Zhang Q M 2010 *Adv. Funct. Mater.* **20** 3266–71
- [26] Liu S, Liu W, Liu Y, Lin J-H, Zhou X, Janik M J, Colby R H and Zhang Q 2010 *Polym. Int.* **59** 321–8
- [27] Chen I-W P, Yang M-C, Yang C-H, Zhong D-X, Hsu M-C and Chen Y 2017 *ACS Appl. Mater. Interfaces* **9** 5550–5
- [28] Terasawa N 2017 *RSC Adv.* **7** 2443–9
- [29] Wu G, Hu Y, Zhao J, Lan T, Wang D, Liu Y and Chen W 2016 *Small* **12** 4986–92
- [30] Mukai K, Asaka K, Kiyohara K, Sugino T, Takeuchi I, Fukushima T and Aidab T 2008 *Electrochem. Acta* **53** 5555–62
- [31] Akle B J and Leo D J 2007 *Smart Mater. Struct.* **16** 1348–60
- [32] Akle B J and Leo D J 2012 *Smart Mater. Struct.* **21** 105034

- [33] Akle B, Nawshin S and Leo D 2007 *Smart Mater. Struct.* **16** S256–61
- [34] Akle B J, Habchi W, Wallmersperger T, Akle E J and Leo D J 2011 *J. Appl. Phys.* **109** 074509
- [35] Kruusamäe K, Sugino T and Asaka K 2015 *J. Appl. Phys.* **118** 014502
- [36] Nakshatharan S, Punning A, Johanson U and Aabloo A 2018 *J. Appl. Phys.* **123** 014502
- [37] Palmre V, Lust E, Jänes A, Koel M, Peikolainen A-L, Torop J, Johanson U and Aabloo A 2011 *J. Mater. Chem.* **21** 2577–83
- [38] Palmre V, Brandell D, Mäeorg U, Torop J, Volobujeva O, Punning A, Johanson U, Kruusmaa M and Aabloo A 2009 *Smart Mater. Struct.* **18** 095028
- [39] Kornyshev A A, Twidale R M and Kolomeisky A B 2017 *J. Phys. Chem. C* **121** 7584–95
- [40] Biesheuvel P M and Bazant M Z 2010 *Phys. Rev. E* **81** 031502
- [41] Biesheuvel P M, Fu Y and Bazant M Z 2011 *Phys. Rev. E* **83** 061507
- [42] Neugebauer S, Mller U, Lohmller T, Spatz J P, Stelzle M and Schuhmanna W 2006 *Electroanalysis* **18** 1936
- [43] Zhang B, Zhang Y and White H S 2004 *Anal. Chem.* **76** 6229–38
- [44] Sanginov E, Kayumov R, Shmygleva L, Lesnichaya V, Karelin A and Dobrovolsky Y 2017 *Solid State Ion.* **300** 26–31
- [45] Schmidt C, Glück T and Schmidt-Naake G 2008 *Chem. Eng. Technol.* **31** 13–22
- [46] Landau L D and Lifschitz E M 1986 *Theory of Elasticity* 3rd edn (Oxford: Pergamon)
- [47] Öz H R and Özkaya E 2005 *Math. Comput. Appl.* **10** 369–76
- [48] Daikhin L I, Kornyshev A A and Urbakh M 1996 *Phys. Rev. E* **53** 6192–9
- [49] Goldstein R E, Pesci A I and Romero-Rochín V 1990 *Phys. Rev. A* **41** 5504–15
- [50] Bilby B A 1950 *Proc. Phys. Soc. A* **63** 191–200
- [51] Cha Y, Verotti M, Walcott H, Peterson S D and Porfiri M 2013 *Bioinsp. Biomim.* **8** 036003
- [52] Anand S V, Arvind K, Bharath P and Mahapatra D R 2010 *Smart Mater. Struct.* **19** 045026
- [53] Brufau-Penella J, Puig-Vidal M, Giannone P, Graziani S and Strazzeri S 2008 *Smart Mater. Struct.* **17** 015009
- [54] Cha Y, Shen L and Porfiri M 2013 *Smart Mater. Struct.* **22** 055027
- [55] Giacomello A and Porfiri M 2011 *J. Appl. Phys.* **109** 084903
- [56] Timoshenko S and Goodier J N 1951 *Theory of Elasticity* 2nd edn (New York: McGraw-Hill)
- [57] Kim O, Shin T J and Park M J 2013 *Nat. Commun.* **4** 2208
- [58] Gere J and Goodno B 2012 *Mechanics of Materials* 8th edn (Oxford: Cengage Learning)